ELECTRIC DRIVING NEGATIVE PRESSURE VARIABLE SUPPLY SYSTEM OF AIR-SUCTION SEED METERING DEVICE

Kexin XU[1], Yin CHEN[2], Tianhao JING[3], Jianqiao WANG[4], Yulong CHEN[5*], Meng ZHANG[6]

The negative pressure fan serves as a critical component in the air-suction seed metering device. Current implementations predominantly employ fans maintaining constant maximum wind speeds during operation, leading to substantial energy inefficiencies. To address this limitation, this study introduces an intelligent pressure regulation system utilizing a DC brushless negative pressure fan controlled through an ICAN7404 module coupled with microcontroller-based adaptive control. Experimental results demonstrate responsive system performance with average rise and settling times of 1123.58 ms and 1144.75 ms respectively. The control system achieved exceptional stability metrics, maintaining an average steady state error of 95.69 $r \cdot min^{-1}$ with 0.53% overshoot. Comparative analysis reveals significant advantages in energy efficiency and operational consistency over conventional constant-speed systems. This electromechanical control framework advances precision agriculture technology by enabling dynamic pressure adaptation to actual seeding requirements. This study can provide a reference for the electric driving pressure supply technology of the seed metering device.

[1] College of Agricultural Engineering and Food Science, Institute of Modern Agricultural Equipment, Shandong University of Technology Zibo, 255000, China, e-mail: 2536570601@qq.com
[2]College of Agricultural Engineering and Food Science, Shandong University of Technology, Zibo, 255000, China, e-mail: 2874194730@qq.com
[3]College of Agricultural Engineering and Food Science, Shandong University of Technology, Zibo, 255000, China, e-mail: 18353169398@163.com
[4]College of Agricultural Engineering and Food Science, Shandong University of Technology, Zibo, 255000, China, e-mail: 19811709920@163.com
[5]College of Agricultural Engineering and Food Science, Institute of Modern Agricultural Equipment, Shandong University of Technology, Zibo, 255000, China, e-mail: cyl06471@sdut.edu.cn
[6]Weichai Leiwo Intelligent Agriculture Technology Co, Weifang, 261206, China, e-mail: 411225919@qq.com

Keywords: the negative pressure fan; CANopen communication; air-suction seed metering device

1. Introduction

The air-suction seed metering device uses a negative pressure fan to create vacuum in the air chamber, adsorbing seeds through suction holes for seed pickup [1]. However, the negative pressure fan is mostly driven by the power output shaft of tractor, and its high speed can ensure normal operation of the seed metering device [2], resulting in energy consumption [3].

The 5000 pneumatic precision seeder developed by Secole in the United States uses a hydraulic motor to drive a negative pressure fan. Under different operation speeds, the seeding accuracy and [4] are improved through a stable negative pressure of the fan. Yatskul et al. designed an airflow distributor for the centrifugal fan on the seeder [5]. Through the transverse distribution of the airflow by the distributor, the wind speed at the outlet of the fan is more uniform and the accuracy of the transverse distribution of the airflow is improved. Through CFD simulation, Lee et al. studied the law between fan characteristics and parameters such as blade load distribution and impeller profile, and finally determined the parameter combination through experiments, which significantly enhanced the overall performance of the fan [6]. Wang Feng simulated with Fluent software [7], obtained the performance curve of the fan, established mathematical models of different factors-performance indicators, optimized the fan structure of the air suction seeder, and improved the working efficiency and stability of the fan. Qi Dongda et al. used Ansys software to couple the Francis fan [8], the impact of different parameters on the performance of the fan, and the number of guide vanes and flow rate when the performance of the fan is obtained. Li Hui et al. used CFD numerical simulation [9] to study the internal flow field and external characteristics of the fan, and obtained the number of blades when the overall performance of the centrifugal fan is better. Luo Kai et al. used Fluent software to simulate the three-dimensional value of the fan [10] to study the influence of the size parameters of the fan on its flow noise and air volume.

This study focused on the development of specialized electric driving negative pressure fan for air-suction seed metering devices, aiming to achieve variable negative pressure supply while ensuring seeding quality and reducing fan power consumption. A brushless DC negative pressure fan was employed to generate vacuum for the air-suction seed metering device. Communication with the master station was realized using an ICAN7404 module. Experimental investigations were conducted to analyze the relationships between fan duty cycle, rotational speed, negative pressure, and current. High-speed camera imaging was utilized to capture and analyze seed aspiration states during seed detachment from

the population. A mathematical model correlating operational speed with fan rotational speed was established. The Kalman filter algorithm was applied to enhance the accuracy of fan rotational speed. Subsequently, a segmented incremental PI control algorithm was implemented to enable dynamic adjustment of fan speed according to operational speed variations, thereby achieving variable negative pressure supply. Finally, experimental analyses were performed to evaluate the control effectiveness of fan speed regulation.

2.Materials and Methods

2.1 Selection and design of system hardware

This system used the CANopen communication protocol and relied on the CAN communication conversion module to communicate with STM32. Functions of system included: fan speed control, fan actual speed reading, and fan negative pressure reading. CAN communication conversion modules selected ICAN3402 and ICAN7404, set the node addresses in CAN communication to 4 and 5 respectively. Analog input and digital output functions of the ICAN3402 module were mainly used. The digital input of the ICAN7404 module had functions such as counting, frequency measurement, and PWM measurement. The transmission on different channels was about 200 kHz. When the corresponding digital input channel was counting, the digital output channel output PWM up to 50 kHz.

Referring to researches on the seeding performance of the high-speed precision
air-suction maize seed metering device [11-16], when the operation speed is 12 $km \cdot h^{-1}$, the working negative pressure is 4.0 kPa. The negative pressure variable supply system used WS4235B-12-210-S100-BZJ01 DC brushless negative pressure fan with a rated voltage of 12 V, a rated power of 144 W, a maximum working negative pressure of 5.5 kPa, a maximum speed of 24000 $r \cdot min^{-1}$, an air volume of 80 $m^3 \cdot h^{-1}$, and the supporting used of WS2815DY01V01-SRP004 Negative pressure fan driver. The MCP-H10-B200KPPN air pressure sensor was selected to measure wind pressure.

The overall design idea of the system is shown in Fig.1. The WS2815DY01V01-SRP004Y01V01-SRP004 negative pressure fan driver is used to drive the WS4235B-12-210-S100-BZJ01-12-210-S100-BZJ01 DC brushless negative pressure fan. The fan outlet is connected to the MCP-H10-B200KPPN air pressure sensor. The output voltage of the air pressure sensor is transmitted to the STM32 through the ICAN3402 module. The STM32 microcontroller outputs PWM, and the serial port assistant outputs the fan speed and air pressure sensor voltage to realize variable supply of negative pressure.

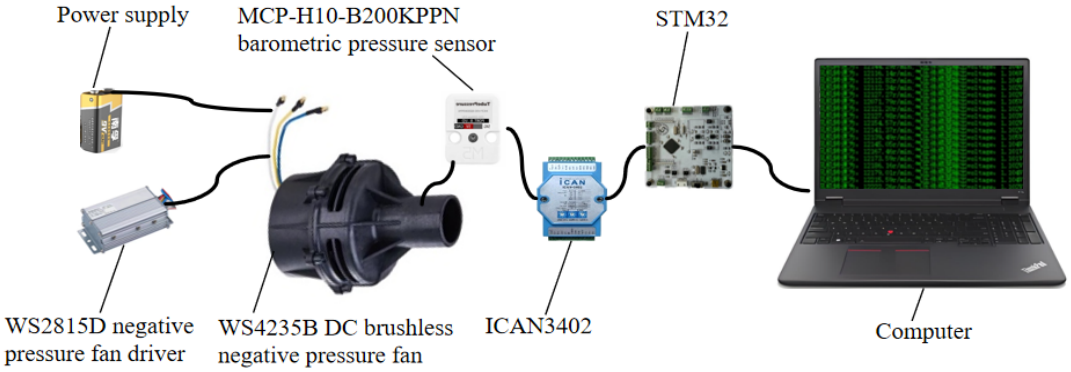

Fig.1 The overall design idea diagram of the system

2.2 Readout the actual rotational speed of fan

The magnetic poles of fan are two pairs, so the fan rotates one circle to output two pulses. The fan is directly controlled by the potentiometer to work at a certain speed, as shown in Fig.2, and the oscilloscope is used to capture the speed pulse of 0.5-4.47 V square wave.

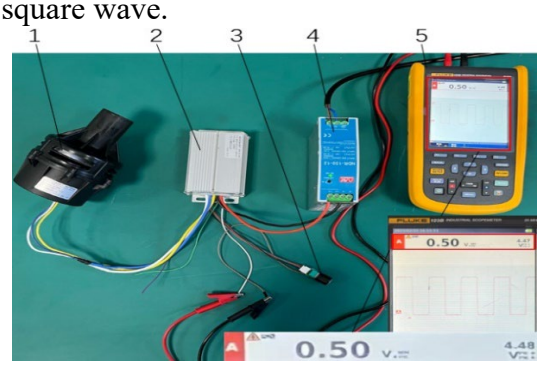

Fig.2 Measure characteristics of fan speed pulse signal 1. Negative pressure fan 2. fan driver 3. potentiometer 4. DC power supply 5. Oscilloscope

The process involves configuring the digital input channel EINO of the ICAN7404 module into counter mode, utilizing the timer interrupt and counter reset operation of the STM32 microcontroller. This enables counting square wave signals within a unit time period and subsequent re-counting, thereby achieving actual fan speed calculation for the fan. The workflow is illustrated in Fig.3.

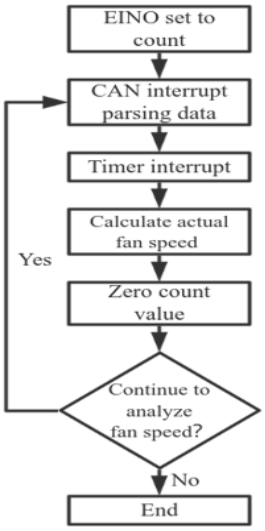

Fig.3 Analysis workflow of the actual fan speed

2.3 Kalman filter algorithm

The actual fan speed is measured by ICAN7404 digital input function. Due to the influence of CAN communication rate, timer and interrupt priority, the measurement accuracy of actual fan speed is low, which affects the closed-loop control accuracy of fan speed. Therefore, the first-order Kalman filter algorithm is used to realize the filtering of actual fan speed. Based on the idea of optimal digital recursion, the filtering algorithm gives different weights to the predicted value and the measured value, and then obtains the revised value.

Prediction system covariance equation:

$$P_K^- = P_{K-1} + Q \tag{1}$$

where

P_K^-, the systematically estimated covariance at time *K*;

P_{K-1}, the systematically covariance at time *K-1*;

Q, the process noise covariance.

Kalman gain equation:

$$K_k = \frac{P_K^-}{P_K^- + R} \tag{2}$$

where

K_k, the kalman gain;

R, the observation noise covariance.

Updated optimal estimator equation:

$$X_k = X_{k-1} + K_k(Z_k - X_{k-1}) \tag{3}$$

where

X_k, X_{k-1},the optimal estimated value of fan speed at time k and $k-1$;

Z_k, measured value of fan speed.

Updated covariance equation:

$$P_k = (1 - K_k)P_K^- \tag{4}$$

where

P_k, the covariance of the system at time k.

After debugging tests, when filtering different fan speeds, P_{k-1}, X_{k-1}, Q and R are set to 0.01, 2000, 10.5, 55 respectively. The change curve before and after filtering when the fan speed around 4200-4450 r·min^{-1} is shown in Fig.4.

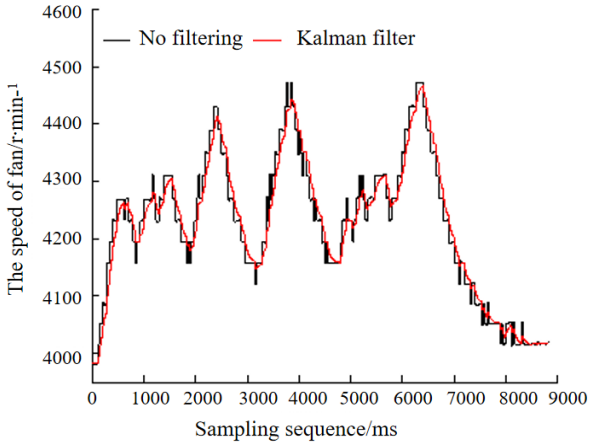

Fig.4 The change curve of fan speed before and after filtering

2.4 Incremental PI algorithm of fan speed

The closed-loop control of the fan speed uses incremental PI algorithm, the control principle is shown in Fig.5, where F _ target _ speed is the target fan speed, F _ real _ speed is the actual fan speed.

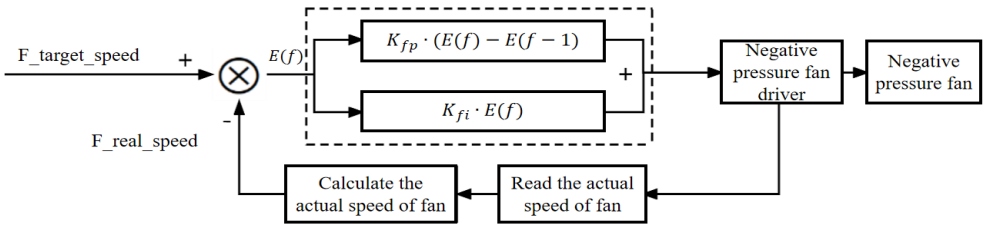

Fig.5 Fan speed incremental PI algorithm control schematic diagram

The incremental PI algorithm formula of fan speed:

$$\Delta V_f = K_{fp}[E(f) - E(f-1)] + K_{fi}E(f) \quad (5)$$

where

ΔV_f, the dynamic change amount of incremental PI control output of fan speed at two adjacent moments;

$E(f)$, difference between the fan target speed and actual speed at time *f*;

$E(f-1)$, difference between fan target speed and actual speed at time *f-1*;

K_{fp}, K_{fi}, the proportional and integral term coefficients in closed-loop

2.5 Software design for air pressure sensor-negative pressure fan

ICAN3402 analog input pin AI0 is used to read the voltage output by air pressure sensor, then transmit the voltage value to the main station STM32 microcomputer via TPDO. The voltage signal is further parsed in CAN receive interrupt, and finally the data is displayed in a serial port assistant for later analysis. The implementation process is shown in Fig.6.

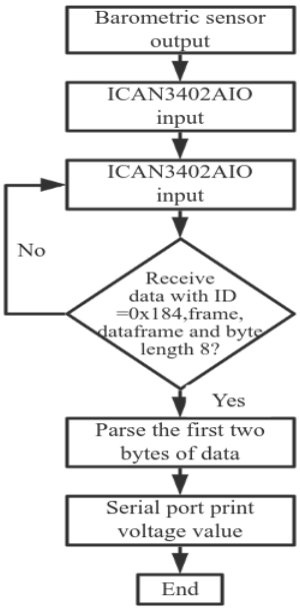

Fig.6 Analysis of pressure sensor voltage value

To accurately measure the working negative pressure of the fan, the air pressure sensor calibration test was carried out. During the experiment, STM32 microcontroller generated PWM signals to incrementally raise the negative pressure

of the fan at 0.1 kPa intervals. The voltage of pressure sensor was sent to STM32 via the ICAN3402 module. Real-time fan speed was calculated using input capture, while a multimeter measured the operating voltage at varying speeds. A serial port assistant then output the fan speed and sensor voltage data, enabling pressure sensor calibration and performance analysis of negative pressure fan, as shown in Fig.7.

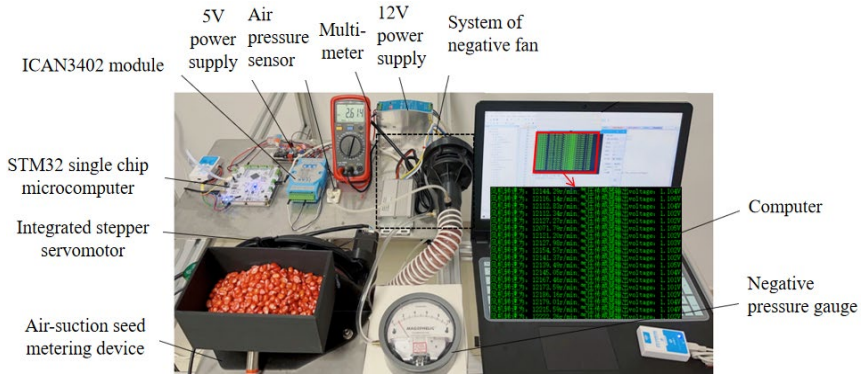

Fig.7 Pressure sensor calibration and fan characteristics exploration test

Origin software is used to process the results to obtain the output voltage of the air pressure sensor and the negative pressure of the negative pressure meter, as well as the relationship between fan speed, negative pressure and current intensity. As shown in Fig.8, the voltage of pressure sensor decreases with rising negative pressure. Calibration improved its accuracy from 1.5 kPa to 0.1 kPa, Eq.6 provided a basis for setting target fan speeds at different operation speeds. The relationship between fan speed and current intensity is shown in Fig.9, and Eq.7 links fan speed to current intensity (11.04 A at maximum speed).

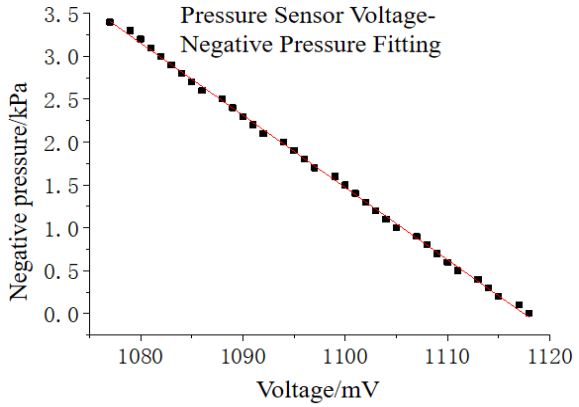

Fig.8 Characteristics of air pressure sensor and negative pressure fan

The functional relationship between the output voltage value of air pressure sensor and measured negative pressure value:

$$P = -0.084U + 94.072, R^2 = 0.99917 \quad (6)$$

Where P, the negative pressure value measured by the air pressure sensor, kPa;

U, the output voltage value of the air pressure sensor, mV.

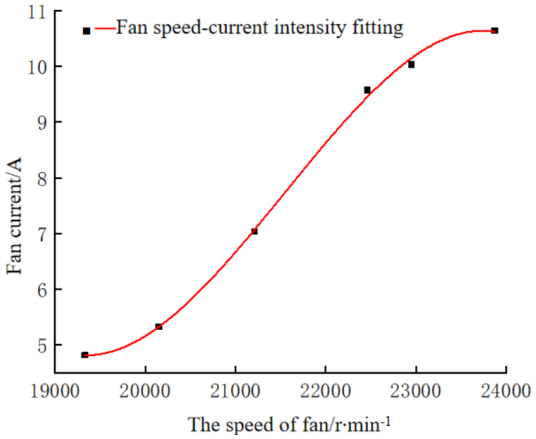

Fig.9 Relationship between fan speed and current intensity

Functional relationship between fan speed and current intensity:

$$I = -1.38N_f^3 + 8.94N_f^2 - 0.19N_f + 1347.94, R^2 = 0.99768 \quad (7)$$

where

I, the current intensity of the fan, A;

N_f, the rotational speed of the fan, r·min^{-1}.

3. Experimental Results and Discussion

3.1 Best fan speed test

To study the optimal fan speed matching different operation speeds while ensuring seeding performance, with the aim of minimizing fan speed and thereby reducing overall system power consumption, a mathematical model of working speed versus fan speed was established. This model serves as the target fan speed in the incremental PI algorithm for fan speed control. The experimental setup (shown in Fig.10) consists of an air-suction seeding system, high-speed camera system, oscilloscope, STM32 microcontroller, and power supply system. The air-suction seeding system includes a suction-type seed meter, integrated stepper servo motor, and negative pressure fan. The high-speed camera system comprises a FASTCAM Mini camera (Nikon lens), fill light, and a computer equipped with Photron FASTCAM Viewer image processing software. The power supply system incorporates 12 V, 12 V to 24 V boost, and 12 V to 5 V step-down modules.

Zhengdan958 (a maize cultivar) maize seeds were used in test, the plant spacing was 250 mm, and the working speeds were 2, 4, 6, 8, 10, 12 km·h^{-1}, respectively. When the seed metering device works at different working speeds, the STM32 single chip microcomputer output PWM, and the fan speed was gradually increased from 17000 r·min^{-1} to 24000 r·min^{-1} at an interval of 1000 r·min^{-1}, and the fan speed was verified by oscilloscope. The high-speed camera was used to photograph the aspiration state of seeds about to enter the seed carrying stage. 251 maize seeds were continuously repeated for three times, and the aspiration rate of single seed was averaged. When the operation speed is 12 km·h^{-1} and the fan speed is 24000 r·min^{-1}, the single particle aspiration rate was 93.5%. Based on the single particle aspiration rate of 93.5%, the fan speed at the operation speed was 2, 4, 6, 8, 10, 12 km·h^{-1} respectively.

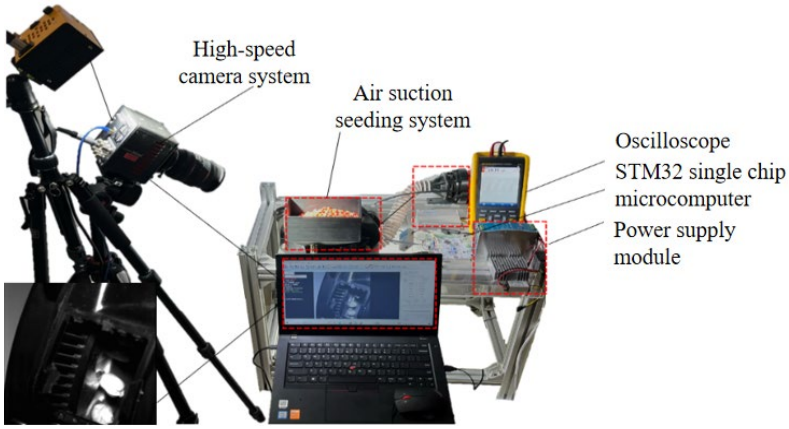

Fig.10 Exploring the best fan speed bench test

The test results are processed by Origin software, as shown in Fig.11. The polynomial fitting curves of fan speed-single particle aspiration rate at different operation speeds are obtained, and the formula is shown in Eq.8.

$$\begin{cases} \delta_2(N_f) = -8.83 \times 10^{-7} N_f^2 - 0.04 N_f - 344.70 \\ \delta_4(N_f) = -1.20 \times 10^{-6} N_f^2 - 0.53 N_f - 495.30 \\ \delta_6(N_f) = -1.88 \times 10^{-6} N_f^2 - 0.08 N_f - 857.85 \\ \delta_8(N_f) = -1.41 \times 10^{-6} N_f^2 - 0.07 N_f - 735.41 \\ \delta_{10}(N_f) = -1.36 \times 10^{-6} N_f^2 - 0.07 N_f - 776.26 \\ \delta_{12}(N_f) = -1.17 \times 10^{-6} N_f^2 - 0.06 N_f - 709.71 \end{cases} \tag{8}$$

Where N_f, the fan speed, r·min^{-1}; $\delta_i(N_f)$, the single particle aspiration rate, %;
i, the value of operation speed, km·h^{-1}.

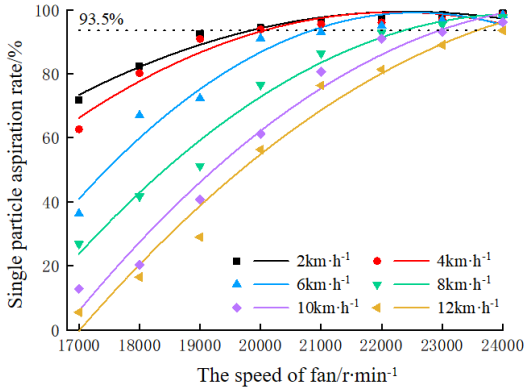

Fig.11 Fitting curve of fan speed and single particle aspiration rate

When the single particle aspiration rate is 93.5%, the corresponding fan speeds are 19328.91, 20147.42, 21211.50, 22457.41, 22947.16, 23872.42 r·min^{-1}. Polynomial fitting is performed on the operation speed and fan speed, as shown in Fig.12, and the fitting polynomial is shown in Eq.9.

$$N_f = -7.87V^2 + 572.55V + 18130.61, R^2 = 0.98771 \quad (9)$$

Where N_f, the fan speed, r·min^{-1}; V, the operation speed, km·h^{-1}.

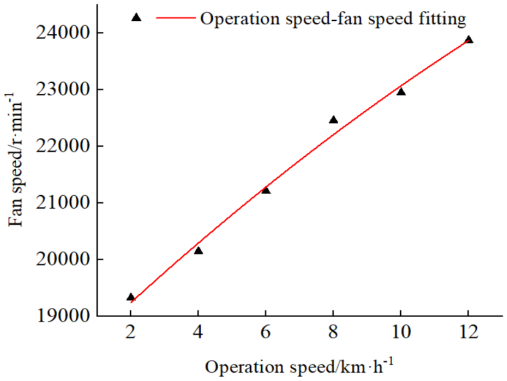

Fig.12 Fitting curve of operation speed and fan speed

3.2 Closed loop control test of fan speed

Under different operation speeds, the target fan speed is obtained from the mathematical model of operation speed-fan speed. First, when the operation speed is set to 2 km·h^{-1}, the target fan speed is 19328.91 r·min^{-1}, and the incremental PI control parameters of the fan speed are adjusted. The proportional term and integral term in incremental PID are equivalent to the differential term and proportional term in positional PID. Positional PID is applied in incremental PI according to the step parameters of proportional term, integral term, differential term. It should be

integral term first, then proportional term, and determine K_{fi} and K_{fp} in sequence. When K_{fi}, let K_{fp} be 0, make K_{fi} take a value within 0.02-0.07, and the interval is 0.01, and get the K_{fi} value of the response characteristics. When K_{fp}, K_{fi} remains unchanged, so that K_{fp} takes a value within 0.30-0.34, with an interval of 0.01, and then the K_{fp} value of the response characteristic is obtained. Through this, the K_{fi} and K_{fp} values of the system response characteristics are determined when the target fan speed is 19328.91 r·min^{-1}.

Taking the above K_{fi} and K_{fp} values as the initial values of the fan speed incremental PI control when the fan target speed is 20147.42, 21211.50, 22457.41, 22947.16, 23872.42 r·min^{-1}, the system response characteristics under different fan speeds. If the control effect of this set of parameters is close to the target speed of different fans, then this set of parameters will be used as the incremental PI control parameters of the entire fan speed. Otherwise, the K_{fi} and K_{fp} values need to be further different to achieve different fan target speeds. Speed incremental PI control can achieve better control effects. The fan speed incremental PI algorithm parameter tuning step response curve is shown in Fig.13 and Fig.14.

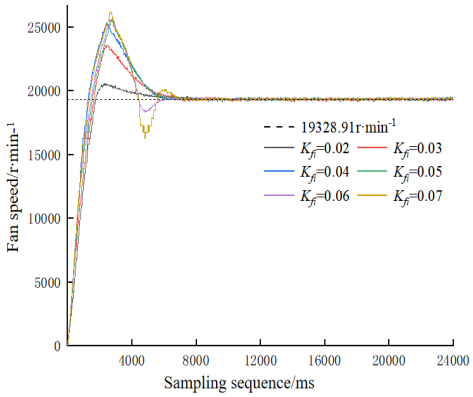

Fig.13 Step response curve of fan speed when K_{fp}=0 and K_{fi}=0.02-0.07

Table 1

Step response result of fan speed when K_{fp}=0 and K_{fi}=0.02-0.07

K_{fi}	Δt_r, ms	ΔT, ms	e_{ss}, r·min^{-1}	OS, %
0.02	1862	5428	152.06	6.15
0.03	1651	6143	136.42	16.52
0.04	1240	5857	109.16	20.45
0.05	1524	6025	112.82	23.22
0.06	1416	6358	118.36	25.44
0.07	1313	6858	124.04	26.20

It can be seen from Fig.13 and Table 1 that the OS increases as K_{fi} increases, reaching a maximum of 26.20% when K_{fi} *equals* 0.07. When K_{fi} equals 0.04, the minimum e_{ss} (steady state error) is 109.16 r·min^{-1}, which increases time first decreases, then increases and then decreases the trend is obtained. When K_{fi} *equals* 0.04, the minimum Δt_r (rising time) is 1240 ms. Due to the large fan speed, ΔT (adjustment time) is greater than 5000 ms when K_{fi} is between 0.02 and 0.07. Therefore, the comprehensive response characteristics of the system are relative when K_{fi} *equals* 0.04.

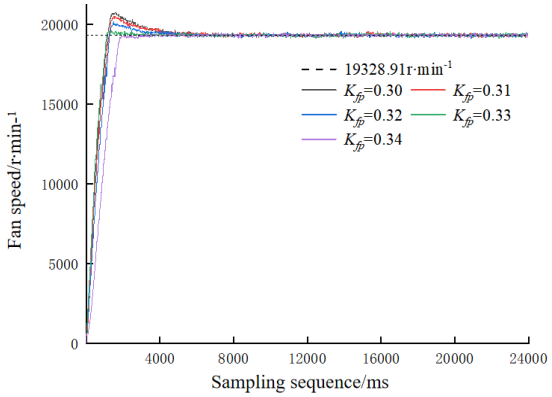

Fig.14 Step response curve of fan speed when K_{fi}=0.04 and K_{fp}=0.30-0.34

Table 2

Step response result of fan speed when K_{fi}=0.04 and K_{fp}=0.30-0.34

K_{fi}	Δt_r, ms	ΔT, ms	e_{ss}, r·min^{-1}	OS, %
0.30	1115	5661	107.61	7.28
0.31	1167	5078	103.24	5.79
0.32	1192	3461	100.82	3.67
0.33	1042	1065	98.42	1.17
0.34	3320	3382	105.75	0.86

To shorten ΔT, reduce e_{ss}, and suppress OS (overshoot), a proportional link is added Fig.14 and Table 2 show that the inhibitory effect on OS increases with the increase of K_{fp}. When K_{fp} equals 0.33-0.34, the OS is less than 3%. At the same time, the e_{ss}, Δt_r and ΔT also show a trend of first decreasing and then increasing. When K_{fp} is 0.33, the minimum e_{ss} is 98.42 r·min^{-1}, and the Δt_r and ΔT are 1042 ms and 1065 ms respectively. Therefore, when K_{fi} equals 0.04 and K_{fp} equals 0.33, the system responds quickly, ΔT, e_{ss} and OS are small.

K_{fp} *equals* 0.33 and K_{fi} *equals* 0.04 are set to the initial values for incremental PI control of other fan target speeds. Under different step inputs, it can be seen from

Table 3 that compared with the response characteristics when the target speed is 19328.91 r·min^{-1}, except that the response characteristics change little when the target speed is 20147.42 r·min^{-1}, other target speed response characteristic parameters all show an increasing trend.

Table 3

Response result of fan speed at different operation speeds when K_{fi}=0.04 and K_{fp}=0.33

Fan speed, r·min^{-1}	Δt_r, ms	ΔT, ms	e_{ss}, r·min^{-1}	OS, %
19328.91	1042	1065	98.42	1.17
20147.42	1057	1075	102.26	1.32
21211.50	1172	4708	113.21	3.93
22457.41	1225	3574	117.52	4.52
22947.16	1274	6270	126.74	5.02
23872.42	1326	5192	121.36	5.09

Therefore, this set of parameters is only applicable when the fan target speed is 19328.91-20147.42 r·min^{-1}. When fan target speed increases, better K_{fp} and K_{fi} values should be selected.

3.3 Optimization test of fan speed

To ensure the fan speed has stable response performance in different ranges, segmented incremental PI control is used to optimize the system to shorten ΔT and suppress OS. The target speeds are set to 19328.91-20147.42, 21211.50-22457.41, 22947.16-23872.42 r·min^{-1}. Within the setting range of the three groups of target speeds, each pass trial and error method The quantitative PI adjustment parameters are finally determined to be unchanged within the target speed range of 19328.91-20147.42 r·min^{-1}, and the parameters Kfp and Kfi within the target speed range of 21211.50-22457.41, 22947.16-23872.42 r·min^{-1} are: 0.35, 0.04 and 0.37, 0.05 respectively. the system adopts segmented incremental PI control The optimized step response curves of different fan speeds are shown in Fig.15.

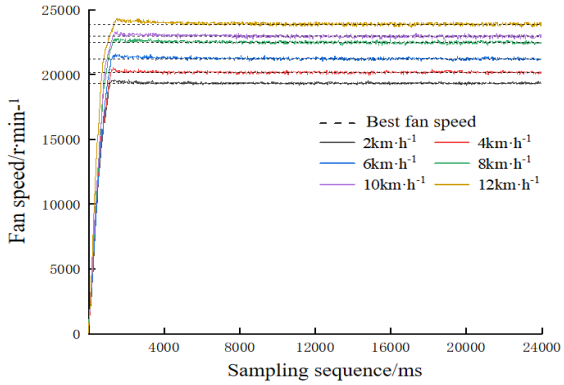

Fig.15 Response curve of fan speed under different operation speeds after optimization

Table 4

Response results of fan speed under different operation speeds after optimization

Fan speed, r·min^{-1}	Δt_r, ms	ΔT, ms	e_{ss}, r·min^{-1}	OS, %
19328.91	1042	1065	98.42	1.17
20147.42	1057	1075	102.26	1.32
21211.50	1069	1082	108.35	1.25
22457.41	1085	1116	106.22	1.22
22947.16	1106	1143	119.08	1.19
23872.42	1135	1158	115.86	1.53

It can be seen from Fig.14 and Table 4 that the target speed of the fan is within 21211.50-22457.41 r·min^{-1} and 22947.16-23872.42 r·min^{-1}, and the average Δt_r and ΔT are 1077 ms, 1120.5 ms and 1099 ms, 1150.5 ms respectively. Compared with before optimization, the average Δt_r are 121.5 ms and 179.5 ms respectively. The average ΔTs are 3042 ms and 4580.5 ms respectively. The average e_{ss} and OS are 107.29 r·min^{-1}, 117.47 r·min^{-1} respectively, 1.24% and 1.36%. Compared with before optimization, the average e_{ss} is 8.08 r·min^{-1} and 6.58 r·min^{-1} respectively. The average OSs are 2.99% and 3.70% respectively. Therefore, the segmented incremental PI control enables the fan to have a better response effect in different operation speed ranges.

3.4 Dynamic response test of fan speed

To explore the dynamic response performance of the motor speed when the operation speed changes, a laboratory simulation experiment was conducted on the following performance of the fan speed and the operation speed. Different operation speeds were sent through the human-computer interaction module so that the

operation speed was between 2-12 km·h^{-1}. Stepwise acceleration and deceleration changes are performed at intervals of 2 km·h^{-1}. The actual rotation speed of the fan at different operation speeds is output through the computer software vofa+, and the response curve is obtained using the Origin software results, as shown in Fig.16. PI control enables the fan to have a better response effect in different operation speed ranges.

It can be seen from Fig.16 and Table 5 that when the system operation speed gradually increases at intervals of 2 km·h^{-1}, the average Δt_r, ΔT, e_{ss} and OS of fan speed are 1213.33 ms, 1231.17 ms, 106.43 r·min^{-1} and 0.67% respectively, and the difference is 169.48 ms, 170.21 ms, 7.18 r·min^{-1} and 0.31%. When the operation speed of the system decreases at intervals of 2 km·h^{-1}, the average Δt_r, ΔT, e_{ss} and OS of fan speed are 1033.83 ms, 1058.33 ms, 84.96 r·min^{-1} and 0.39% respectively, and the difference is 385.32 ms, 396.36 ms, 38.38 r·min^{-1} and 0.19%. Compared with the decrease and increase of working speed, the average Δt_r and ΔT of fan speed are shortened by 179.5 ms and 172.83 ms respectively, and the average e_{ss} and OS are 21.48 r·min^{-1} and 0.29%. It is mainly caused by the fast speed of the fan itself and inconsistent start-up during acceleration and deceleration. In the variable speed operation of the whole system, the average Δt_r and ΔT of the fan speed are 1123.58 ms and 1144.75 ms respectively, and the average e_{ss} and OS are 95.69 r·min^{-1} and 0.53% respectively, so the system has the characteristics of quick response, small difference and high stability.

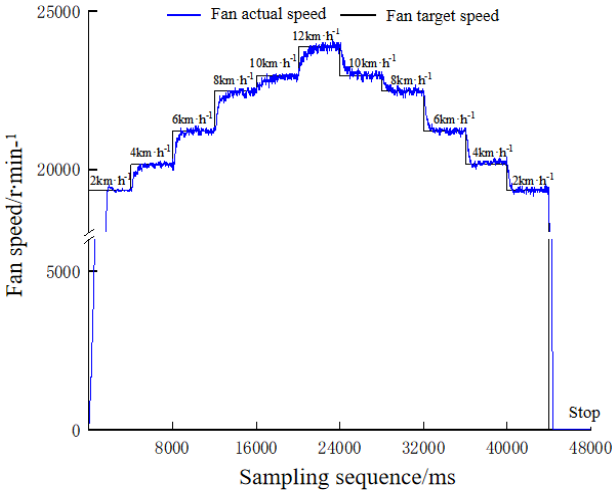

Fig.16 Dynamic response curve of actual fan speed with operation speed

Table 5

Dynamic response results of actual fan speed with operation speed

Type	Operation speed, km·h^{-1}	Target speed of fan, r·min^{-1}	Δt_r, ms	ΔT, ms	e_{ss}, r·min^{-1}	OS, %
Acceleration	0-2	19328.91	1052	1077	93.50	1.35
	2-4	20147.42	1148	1165	101.26	0.52
	4-6	21211.50	1278	1246	107.51	0.64
	6-8	22457.41	1435	1471	112.34	0.55
	8-10	22947.16	975	1005	109.02	0.46
	10-12	23872.42	1392	1423	114.97	0.51
Deceleration	12-10	22947.16	1376	1403	105.63	0.45
	10-8	22457.41	966	993	109.45	0.53
	8-6	21211.50	1325	1364	103.92	0.58
	6-4	20147.42	1223	1252	98.36	0.47
	4-2	19328.91	1083	1108	92.37	0.29
	2-0	0	230	230	0	0

4.Conclusions

(1) Select ICAN7404 and ICAN3402 communication conversion modules to realize CAN communication between the negative pressure variable supply system, the subsequent intelligent seed guidance system and seed metering performance detection system and the STM32 single chip microcomputer of the master station.

(2) Select a DC brushless negative pressure fan to provide negative pressure for the seed metering device and use the air pressure sensor to measure the working negative pressure value of the system, and further calibrate the air pressure sensor and explore the characteristics of the negative pressure fan through tests.

(3) Using high-speed camera shooting, the single-grain aspiration rate of corn seeds when they are about to leave the population and enter the seed-carrying state at the working speed of 2-12 km·h^{-1}, the mathematical model of working speed-fan speed is established, and the fan speed at different working speeds is obtained on the premise of ensuring the stable seeding effect.

(4) The closed-loop control of fan speed is realized by segmented incremental PI algorithm, and the fan speed intervals K_{fp} and K_{fi} are 0.33 and 0.04, 0.35 and 0.04, 0.37 and 0.05, the working speed is 2-12 km·h^{-1}, and the average ΔT, e_{ss} and OS are 1106.5 ms, 108.37 r·min^{-1} and 1.28% respectively in the constant speed and variable speed tests, 1123.58 ms, 95.69 r·min^{-1}, 0.53%, the system has

the characteristics of rapid response, small difference and high stability.

This system can provide stable negative pressure variable supply of air-suction seed metering device at different working speeds, which can provide reference for electric drive pressure supply technology of seed metering device.

REFERENCES

[1] *Liu Tong*. Design and experimental research on air-suction variable aperture precision seed metering device[D]. Shandong: Shandong Agricultural University, 2022.

[2] *Zhang Kaixing* et al. Optimal Design and Experiment of Variable Particle Size Double Disc Air Suction Precision Seed Metering Device [J]. Journal of Agricultural Machinery, 2019, 50 (6): 52-63.

[3] *Lu Jinqing* et al. Optimization design and test of integrated fan of air suction potato planter [J]. Journal of Agricultural Machinery, 2022, 53 (3): 80-90.

[4] *Xu Jianping*, *Xie Yufeng*, *Xu Tao*. Technical status and trend of sowing machinery at home and abroad [J]. Agricultural Mechanization Research, 2011, 33 (2): 234-237.

[5] *Yatskul A*, *Lemiere J P*, *Cointault F*. Influence of the divider head functioning conditions and geometry on the seed's distribution accuracy of the air-seeder[J]. Biosystems Engineering, 2017,161:120-134.

[6] *Lee K K*, *Choi Y S*, *Kim Y L*, et al. Design of axial fan using inverse design method[J]. Journal of Mechanical Science and Technology, 2008,22:1883-1888.

[7] *Wang Feng*. Research on Fan Performance of Air Suction Precision Planter [D]. Heilongjiang: Heilongjiang Bayi Agricultural Reclamation University, 2019.

[8] *Qi Dongda*, *Li Yaogang*, *Dong Jiahao*, et al. Fluid-Structure Coupling Based on ANSYS Workbench Mixed Flow Fan [J]. Mechanical Engineering and Automation, 2018 (2): 67-69.

[9] *Li Hui*, *Wang Jun*, *Zhou Shuiqing*, et al. Influence of blade number on performance of multi-wing centrifugal fan [J]. Fan Technology, 2017, 59 (2): 19-22 47.

[10] *Luo Kai*, *Luo Xin*, *Huang Chuang*, et al. Performance of Multi-wing Centrifugal Fan Based on Fluent [J]. Fluid Machinery, 2014, 42 (7): 25-29.

[11] *Li Yuhuan*, *Yang Li*, *Zhang Dongxing*, et al. Performance analysis and structure optimization of the maize precision metering device with air suction at high-speed condition [J]. Journal of Agricultural Engineering, 2022, 38 (8): 1-11.

[12] *Gábor Milics.* Variable Rate Seeding and Accuracy of Within-Field Hybrid Switching in Maize (Zea mays L.)[J]. Agronomy, 2025, 15.

[13] *Virk S S, Fulton J P, Porter W M, et al.* Row-crop planter performance to support variable-rate seeding of maize[J]. Precision Agriculture, 2020, 21(3).

[14] *Harris G*. Maize Row Spacing and Seeding Rate Informed by Space-per-Plant Geometry[J]. Agronomy, 2025, 15.

[15 *Ahmed K, Saleh A, Musa A, et al.* Determination of selected parameters that influence planting space uniformity on maize seed[J]. Fudma journal of sciences, 2023.

[16] *Petrovi I, Vuajnk F, Trdan S, et al.* The Influence of Planting Speed of a Maize Vacuum Planter on Plant Spacing Variability and Ear Parameters[J]. Agronomy, 2025, 15(2).